Advances in Geo-Energy Research

Vol. 3, No. 1, p. 104-114, 2019
www.astp-agr.com

Original article

Microflow effects on the hydraulic aperture of single rough fractures

Ge Zhang[1,2], Yudong Zhang[1], Aiguo Xu[1,3]*, Yingjun Li[2]

[1]*Institute of Applied Physics and Computational Mathematics, Beijing 100088, P. R. China*

[2]*State Key Laboratory for Geomechanics and Deep Underground Engineering, China University of Mining and Technology, Beijing 100083, P. R. China*

[3]*Center for Applied Physics and Technology, MOE Key Center for High Energy Density Physics Simulations, College of Engineering, Peking University, Beijing 100871, P. R. China*

(Received December 28, 2018; revised January 15, 2019; accepted January 16, 2019; available online January 20, 2019)

Citation:
Zhang, G., Zhang, Y., Xu, A., Li, Y. Microflow effects on the hydraulic aperture of single rough fractures. *Advances in Geo-Energy Research*, 2019, 3(1): 104-114, doi: 10.26804/ager.2019.01.09.

Corresponding author:
*E-mail: xu_aiguo@iapcm.ac.cn

Keywords:
Microflow
single fracture
roughness
hydraulic aperture
lattice Boltzmann method

Abstract:
The understanding of flow behavior in rough fractures is essential for many engineering activities. When the aperture of a rough fracture approaches the mean free path of fluid molecules, the microflow effect, sometimes also referred to relative rarefaction effect, relative discrete effect or non-equilibrium effect, becomes pronounced. It was found often to enhance the flow rate. However, the surface roughness shows completely contrary influence. In order to clarify the influences of the two factors, a computer simulation work accompanied with theoretical analyses is conducted. Previous empirical models for hydraulic aperture which already containing roughness effect are modified with consideration of the microflow effect. Direct simulation using the lattice Boltzmann method is conducted on artificially created 2D fractures with random roughness following Gaussian distribution to reveal the competitive relationship of two effects. The simulation results also verify modified models. Among them, the one based on Rasouli and Hosseinian's model agrees with the simulation on the relationship between hydraulic aperture and mechanical aperture for both cases with very rough fractures and relatively smooth fractures. Further investigation confirms that, under various roughness, the ratio of hydraulic aperture over mechanical aperture shows quantitatively different trends as mechanical aperture decreases. This phenomenon exists on a relatively wide scale. An equilibrium point of two effects is also found through analysis of the relationship. The results reveal the mechanism of microflow in 2D rough fractures and also provide a reference for engineering problems like the transport of natural gas through microfractures.

1. Introduction

Fractures constitute a complex system in rock masses which provides an effective pathway for the fluid flow. However, as fractures are produced both by nature or by human activities with various processes, they diverge on properties and always intersect with each other (Ciezobka et al., 2018; Liu et al., 2018). Therefore, with intricate networks of fractures, it is hard to make an effective prediction for the permeability and other properties of the reservoir. Although discrete fracture network (DFN) models have been widely used to simulate the transport in rock masses and some meaningful results have already been obtained (Cacas et al., 1990; Liu et al., 2017; Golparvar et al., 2018), typically they are based on simplifications on elements of the network by assuming that each single fractures can be explicitly described with a definite permeability model. In this case, researches on single fractures are necessary for it provides the foundation of building a transport process model of rock fractures which can be further implemented into DFN models to improve the accuracy of macroscale prediction (Luo et al., 2016).

For the evaluation of permeability of single fractures, cubic law (CL) is widely used in rock engineering practice. CL is derived in the case of the flow constrained by two smooth plates from the Stokes equation, a simplified form of Navier-Stokes equation (NSE) neglecting inertial term (Witherspoon et al., 1980; Oron and Berkowitz, 1998). However, CL doesn't consider the influence of surface roughness of fractures, while roughness obviously influences the fluid flow and solute transport processes in fractures as a lot of literature has reported (Boutt et al., 2006; Zhao et al., 2018). Attempts

https://doi.org/10.26804/ager.2019.01.09.

have been made to modify CL with roughness factors, among which the mean value and the standard deviation of aperture distribution of fracture were introduced as parameters (Louis, 1972). Adopting the form of CL, modifications can be ascribed to accurate evaluation of hydraulic aperture (e), as shown in Eq. (1):

$$\tilde{Q} = -\frac{e^3}{12\mu}\nabla p \tag{1}$$

where e represents hydraulic aperture and it is a function of mechanical aperture (E), i.e., $f(E,\ldots)$; $\tilde{Q}$ is the flow rate of fracture; μ is the dynamic viscosity of the fluid; and ∇p is the pressure gradient.

One of remarkable works to establish an explicit expression for hydraulic aperture was made by Zimmerman et al. (1991). They built an idealized fracture model with the sinusoidal-shaped surface to study the effect of roughness with lubrication theory in details, and an analytical expression of e was obtained. Under the condition that the wavelength is long and the amplitude is relatively small compared with aperture size, a precise e can be given by their model. In later researches, the ratio between the standard deviation of aperture (σ) and mechanical aperture (E) is used as a parameter for roughness (Zimmerman and Bodvarsson, 1996). Other than this roughness indicator, a number of parameters have also been utilized as quantitative measurements of the roughness. Joint Roughness Coefficient (JRC) (Barton and Choubey, 1977), Z_2 (Myers, 1962) and fractal dimension (Brown, 1995; Cai et al., 2010) are of the most popular ones. Roughness parameters can be introduced to a modified form of e, and a summary of these empirical models has been given in papers (Zhao and Li, 2015; Wang et al., 2016). Due to the ratio of asperity size relatively changes over different E or original distance between two surfaces, nearly all empirical models have included E as a parameter into their model of e, which means the modified aperture is affected not only by roughness property but also by opening state of the fracture. However, as empirical models have little consideration of specific flow details, when E changes, the derived e should be checked carefully before application.

To make a solid investigation on the mechanism of fracture flow, remarkable simulation works have related flow details which are influenced by the morphological pattern of fracture surface with flow conductivity. Also, simulation works can make compensation for experiments with modeling details and without measurement errors. As a simplified form of NSE, Reynolds equation fits for situations with low Reynolds number. Utilizing the Reynolds equation, it is possible to reveal the flow behavior through rough fractures (Liu et al., 2018). However, direct simulation based on NSE is more accurate for capturing flow details at different conditions. Zou et al. (2015) used a wavelet analysis technique to decompose the roughness profile of fracture to several levels, and with a finite-volume direct simulation of NSE, the formation of local eddies was investigated when second-level roughness was included. Their result shows that the secondary roughness mainly causes the dynamic evolution of eddy flow regions, which further impacts the effective flow aperture. Lattice Boltzmann method (LBM) has gained popularity these years which provides an alternative way to directly solve NSE easily, and it is also possible to extend its scopes of application due to the intrinsic advantage inheriting from its physical foundation (Xu et al., 2006a; Li et al., 2018). As to simulations of fracture flow, Eker et al. (2006) used LBM to study a series of synthetic fractures with fractal characters and gave detailed patterns of the flow field. Credible results were further imported to a neural network model, which can make extended predictions for fracture flow in different cases. Through tests of real rock samples, the 3D rough surface of fractures with self-affine property was extracted and decomposed, and LBM simulation reveals the role of different leveled roughness (Wang et al., 2016). With LBM direct numerical simulation, Zhou et al. (2018) analyzed the nonlinear flow behavior in fractures when the sample was sheared. Recent years, with the development of computational science, the cost of direct simulation for fracture flow becomes acceptable, so a lot of issues that have been omitted previously can be approached and investigated in details, but for researches including flow details in previous literature, E is usually kept as a constant and its scaling effect has not been fully investigated.

The heating of exploitation of unconventional resources brings engineers with new challenges, and a prominent one of them is the scaling effect. When E decreases to comparable size of the mean free path of fluid molecules, the Knudsen number (Kn, defined as the ratio of the mean free path over characteristic length, λ/L) may increase and the flow behaviors deviate from the macroscopic conditions; thus microflow effects should be considered. For gas flow in porous media, this issue is well-known as Klinkenberg effect and the deviation from the macroscopic conditions is not a negligible quantity any more (Darabi et al., 2012; Wang et al., 2018). Kn classically divides fluid flow into four regimes: (1) continuum flow regime ($Kn < 0.001$); (2) slipping flow regime ($0.001 < Kn < 0.1$); (3) transition flow regime ($0.1 < Kn < 10$); (4) free molecular flow regime ($Kn > 10$). For continuum flow regime, NSE works well and has been widely used in geo-flows. When the flow steps into slipping regime, NSE still governs the bulk flow, whereas the slipping velocity at the boundary should be considered, which makes the boundary condition inconvenient to deal with. As to the flow in transition regime, NSE is completely invalid and cannot give a correct prediction on flow behavior. Thus it needs comprehensive considerations when handling high Kn flow problems.

Nature fractures and artificially generated fractures commonly exist in strata of different sizes and act as main channels for fluid transport. For specific fluids, it is possible that Kn goes higher than 0.001 when the size of fracture scales down. A higher Kn indicates that the flow will deviate from continuum flow and tend to show microflow behaviors. In addition, the roughness effect still influences the flow. In this case, two remarkable effects coupled with each other. Figuring out the role of two effects is not only meaningful to engineering activities but also with great scientific values.

Motivated by above issues, this paper intends to make an investigation on concerned problems, including: (1) a direct

simulation of fracture flow field to obtain microflow patterns affected by roughness; (2) the role of E which not only affects roughness effect, but also strengthens or weakens microflow effect; (3) the modification of empirical models of hydraulic aperture when microflow effect is taken into consideration and their deviations from direct simulation results. In order to reduce the complexity of modeling and concentrate researches mainly on roughness and microflow effects, 2D fractures are chosen to use in this paper.

2. LBM for microflow simulation

For most cases, NSE governs the flow in single fractures (mass and momentum conservation for incompressible flows):

$$\nabla \cdot \mathbf{u} = 0 \tag{2}$$

$$\frac{\partial \mathbf{u}}{\partial t} + \nabla \cdot (\mathbf{uu}) = -\frac{1}{\rho}\nabla p + \nu \nabla \cdot \left(\nabla \mathbf{u} + (\nabla \mathbf{u})^T\right) \tag{3}$$

Considering microfractures with limited space, fluid flow will slip on the boundary, so a credible method is needed to accurately solve NSE and expediently capture slipping effect (Zou and He, 1997). With a different nature from traditional computational fluid dynamics, LBM provides a path to conveniently make a direct simulation on the fluid flow, which is not only easily implemented but also has an aptitude for extensibility of complex conditions (Xu et al., 2003, 2005, 2006b).

The governing equation of LBM is originated from the Boltzmann equation, which is a basic kinematic conservation equation in statistical physics. Adopting a special discrete form of BGK-Boltzmann equation, LBM can be compared with macroscopic conservation laws through Chapman-Enskog expansion and it retains particle propagation patterns inherited from lattice gas automata (LGA). The evolution equation for LBM reads:

$$\begin{aligned} &f_i(\mathbf{r}+\Delta t\mathbf{e}_i, t+\Delta t) - f_i(\mathbf{r},t) \\ &= -\frac{\Delta t}{\tau + 0.5\Delta t}\left[f_i(\mathbf{r},t) - f_i^{eq}(\mathbf{r},t)\right] \end{aligned} \tag{4}$$

where $f_i(\mathbf{r},t)$ is the particle velocity distribution function, and $f_i^{eq}(\mathbf{r},t)$ is the local equilibrium velocity distribution function. For traditional lattice Boltzmann models, $f_i^{eq}(\mathbf{r},t)$ has an explicit form as the second order truncation of Maxwell distribution (Succi, 2001); $\mathbf{r}$, t, Δx, and Δt are the position, time, space step, and time step, respectively; $\mathbf{e}_i$ is the discretized velocity of fluid micelle, the subscript i represents the index for discrete velocity. For two-dimensional simulation of this work, D2Q9 model with the following discrete velocity is used:

$$\mathbf{e}_i = \begin{cases} (0,0) & i = 0 \\ c\left(\cos\left[\frac{(i-1)\pi}{2}\right], \sin\left[\frac{(i-1)\pi}{2}\right]\right) & i = 1,2,3,4 \\ \sqrt{2}c\left(\cos\left[\frac{(2i-1)\pi}{4}\right], \sin\left[\frac{(2i-1)\pi}{4}\right]\right) & i = 5,6,7,8 \end{cases} \tag{5}$$

where c is the characteristic speed and $c = \Delta x/\Delta t$.

The fluid density (ρ) and velocity ($\mathbf{u}$) are obtained from moments of the distribution function, and the pressure (p) is obtained from the state equation.

$$\rho = \sum_i f_i \tag{6}$$

$$\mathbf{u} = \frac{1}{\rho}\sum_i f_i \mathbf{e}_i \tag{7}$$

$$p = \frac{\rho c^2}{3} \tag{8}$$

The intrinsic property of kinetic boundary conditions has been discussed for flow in microchannels (Zhang et al., 2018a). Flows within the slip regime and marginally within the transition regime can be well described cooperating with a suitable boundary condition. Considering the rough nature of rock surface, diffuse reflection boundary is very suitable for microflow in fractures (Zhao et al., 2016; Wang et al., 2018). Ansumali and Karlin (2002) has derived the discrete form of diffuse reflection boundary condition which has gained popularity in LBM simulation:

$$\begin{aligned} f_i(\mathbf{r}, t+\Delta t) = &\frac{\sum_j \left|(\mathbf{e}_j - \mathbf{u}_w)\cdot \mathbf{n}\right| f_j(\mathbf{r},t)}{\sum_j \left|(\mathbf{e}_j - \mathbf{u}_w)\cdot \mathbf{n}\right| f_j^{eq}(\mathbf{u}_w, \rho_w)} f_i^{eq}(\mathbf{u}_w, \rho_w) \\ &\text{while } (\mathbf{e}_i - \mathbf{u}_w)\cdot \mathbf{n} > 0 \end{aligned} \tag{9}$$

As an indicator for the strength of the non-equilibrium or the microflow effect, a mean Knudsen number ($\overline{Kn}$) is defined for fracture flow as Eq. (10) shows. E is used as characteristic length, and relaxation time in LBM is related to Kn according to Tang et al. (2005).

$$\overline{Kn} = \frac{\lambda}{L} = \frac{\left(\frac{8}{3\pi}\right)^{-0.5}}{N_E \cdot \Delta t}\cdot \tau \approx \frac{\tau \cdot c}{E} \tag{10}$$

Initially, a mesh will be created according to the maximum resolution of the fractures, and then indexes with specified numbers will be attached with mesh grids in order to guide the LBM evolution (as Fig. 1 shows).

In order to stress the microflow effect and combine results with engineering, we select a group of physical parameters of methane gas in the following work. The parameters can be found in Table A-1 in Appendix. Roughness effect coupled with the microflow effect is investigated under different E. A self-developed code is used for simulation, and the code has been well verified in our previous works (Zhang et al., 2017, 2018b).

3. Theoretical analysis of microflow in fractures

Due to the slip velocity caused by the microflow effect commonly exist at boundaries in a microfracture, a global modification can be taken on hydraulic models. If roughness effect singularly influences the flow, a roughness-modified aperture e_r will be derived. The roughness-modified aperture e_r is a function of E and rough parameters, like σ/E, Z_2, JRC, etc. For two-dimensional fully developed flows in a smooth

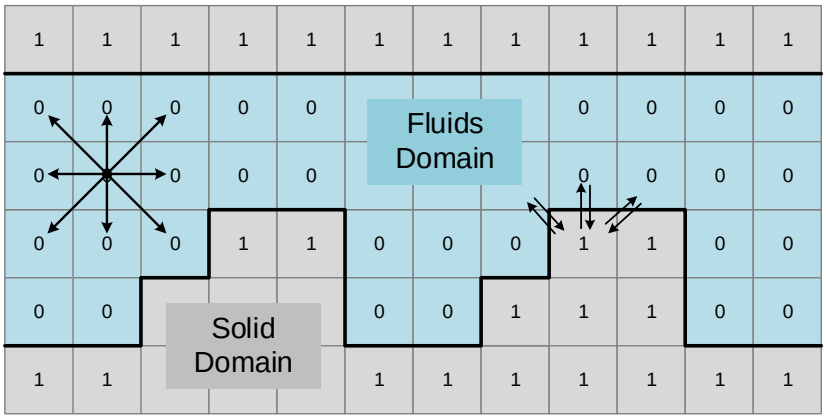

Fig. 1. Binary profile of a 2D fracture for LBM simulation.

channel with a height of e_r, the bulk flow region is governed by NSE. If a second-order slip boundary condition is used:

$$u_{y=0,y=e_r} = \pm A_1 \lambda \frac{\partial u}{\partial y} - A_2 \lambda^2 \frac{\partial^2 u}{\partial y^2} \tag{11}$$

it will lead to the velocity distribution and the flow rate as follows:

$$u(y) = -\frac{e_r^2}{2\mu}\frac{dp}{dx}\left(\frac{y}{e_r} - \frac{y^2}{e_r^2} + A_1\widehat{Kn} + 2A_2\widehat{Kn}^2\right) \tag{12}$$

$$\widetilde{Q} = -\frac{e_r^3}{12\mu}\frac{dp}{dx}\left(1 + 6A_1\widehat{Kn} + 12A_2\widehat{Kn}^2\right) \tag{13}$$

where $\widehat{Kn}$ is the Knudsen number defined by roughness-modified aperture e_r, as λ/e_r.

According to Eq. (1), the expression of e modified both by roughness and the microflow effect is obtained as:

$$e^3 = e_r^3\left(1 + 6A_1\widehat{Kn} + 12A_2\widehat{Kn}^2\right) \tag{14}$$

where A_1, A_2 are coefficients denoting the first-order and the second-order terms of the slip boundary, respectively.

Replace $\widehat{Kn}$ with mean Knudsen number $\overline{Kn}$, we get the form of hydraulic aperture which is a function of E and roughness parameter.

$$e^3 = e_r^3\left(1 + 6A_1\frac{E}{e_r}\overline{Kn} + 12A_2\frac{E^2}{e_r^2}\overline{Kn}^2\right) \tag{15}$$

If $\overline{Kn}$ decreases to 0, the flow is ideally continuum. Then e regress to the roughness-modified one, $e_r = f(E,\ldots)$. As $\overline{Kn}$ increases, the correcting part gets larger, and greater flow rate will be obtained. The value of A_1, A_2 suggested by Karniadakis et al. (2006) is A_1 = 1.0 and A_2 = -0.5, we adopt these two values for the following research as an attempt. Using σ/E as roughness factor, then the explicit expression of the relationship between e and E is shown as Eq. (16):

$$\frac{e}{E} = f\left(\frac{\sigma}{E}\right)\cdot\left(1 + \frac{6A_1\overline{Kn}}{f\left(\frac{\sigma}{E}\right)} + \frac{12A_2\overline{Kn}^2}{f\left(\frac{\sigma}{E}\right)^2}\right)^{\frac{1}{3}} \tag{16}$$

Fig. 2 shows the microflow-modified relationship between e and E. The initial form of selected empirical models is listed in Table A-2 in Appendix (Patir and Cheng, 1978; Renshaw, 1995; Zimmerman and Bodvarsson, 1996; Rasouli and Hosseinian, 2011). Keeping the Knudsen number $\overline{Kn}$ constant, all curves denote that e/E drops with the increase of σ/E (as Fig. 2(a) shows). With a higher value of $\overline{Kn}$, e/E is larger which indicates more fluid transports through the rough fracture. Empirical models are also used to demonstrate the dependence on $\overline{Kn}$ (as Fig. 2(b) shows). With the increase of $\overline{Kn}$, e/E is also getting larger. If a fracture is rougher, with a larger value of σ/E, then e/E becomes lower. The results in Fig. 2 is in accord with our instinct on this problem. However, σ of a fracture is determined by the surface profile and usually stays constant, which means if E changes, it not only causes variances of $\overline{Kn}$, but also leads to differences on σ/E. Therefore, more investigation is needed to reveal the mechanism and confirm the relationship between e and E for microflow conditions.

4. Results and discussion

4.1 Flow field of fractures with random roughness

Neglect waviness of a fracture profile, then only roughness exits on the fracture surface. Ideally, the profile of small-scale roughness statically follows Gaussian distribution, and roughness randomly scatters on the fracture surface (Zou et al., 2015). Due to local aperture (E_x) relates with roughness, one simple and reasonable way to create an ideal rough fracture is to generate E_x randomly. With the value of E and σ, the standard distribution function of E_x is shown as:

$$f(E_x) = \frac{1}{\sqrt{2\pi}\sigma}\exp\left(-\frac{(E_x - E)^2}{2\sigma^2}\right) \tag{17}$$

In order to create a standard profile of ideal rough fractures, a random sampling method is adopted and E_x is generated as Eq. (18) shows. This approach guarantees E_x strictly follows Gaussian distribution function mathematically.

$$E_x = E + \sigma\cdot\sqrt{-2\ln\zeta_1}\cdot\cos(2\pi\zeta_2) \tag{18}$$

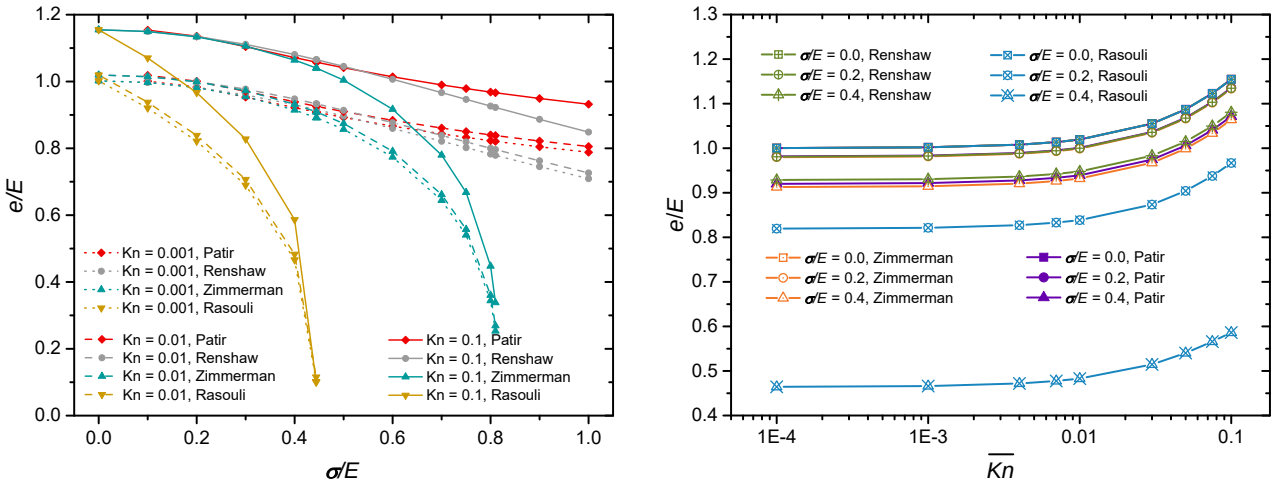

Fig. 2. The microflow-modified empirical models for the hydraulic property (e/E) of single fractures. (a) Relationships between e/E and σ/E; (b) relationships between e/E and $\overline{Kn}$.

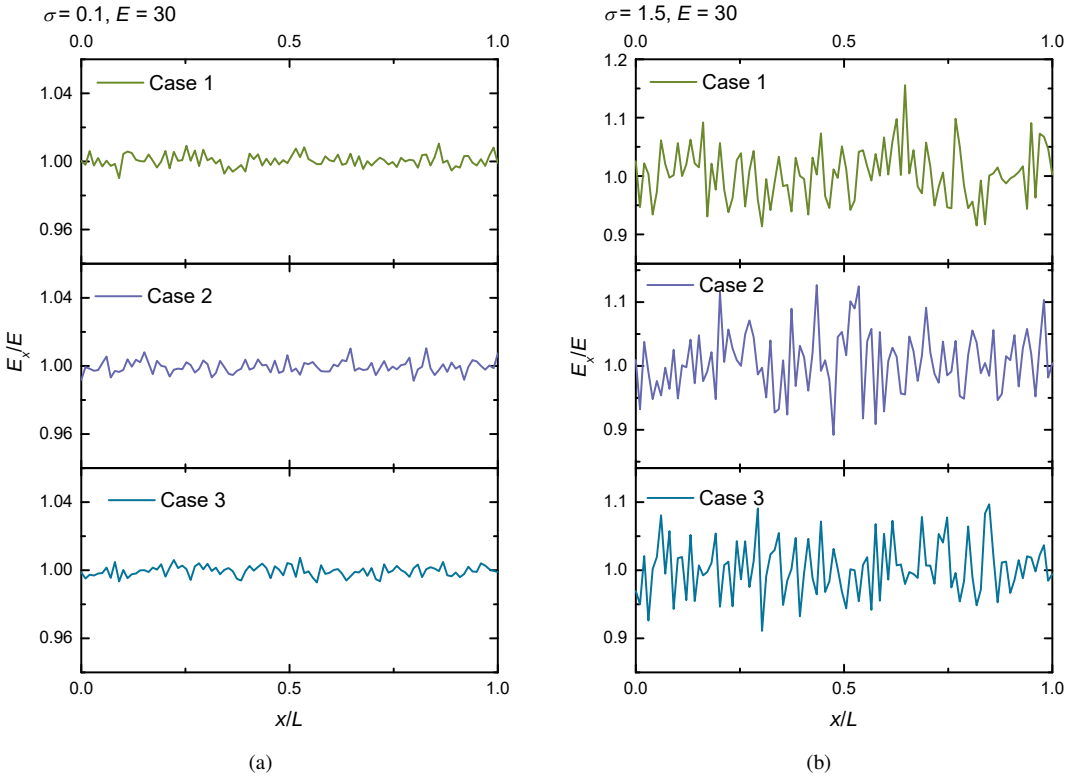

Fig. 3. Rough fractures generated randomly (parameters of σ = 0.1, E = 30 and σ = 1.5, E = 30 are used to produce profiles with 100 sampling seeds, and dimension will be later introduced with the meshing process).

where ζ_1 and ζ_2 are random numbers ranging from 0.0 to 1.0.

Fig. 3 shows randomly generated profiles of six rough fractures. E_x fluctuates around E and the waveform is similar to white noise. These profiles will be imported to the LBM code to demonstration characters of microflow through ideal rough fractures. Two sets of profiles show fractures of relatively smooth and rough conditions. To eliminate the uncertainty, three cases with the same parameter (σ and E) are generated and simulated.

Firstly, the velocity field of one length of fractures from 0.004 to 0.006 m is selected to display. As Fig. 4 shows, flow patterns transform accordingly with the change of E. With a larger aperture, streamlines are smooth and straight. While as E decreases, streamlines near the peak of roughness are torturous, and the velocity distribution is asymmetrical along the x-direction. This is obvious for a rough fracture, but for a

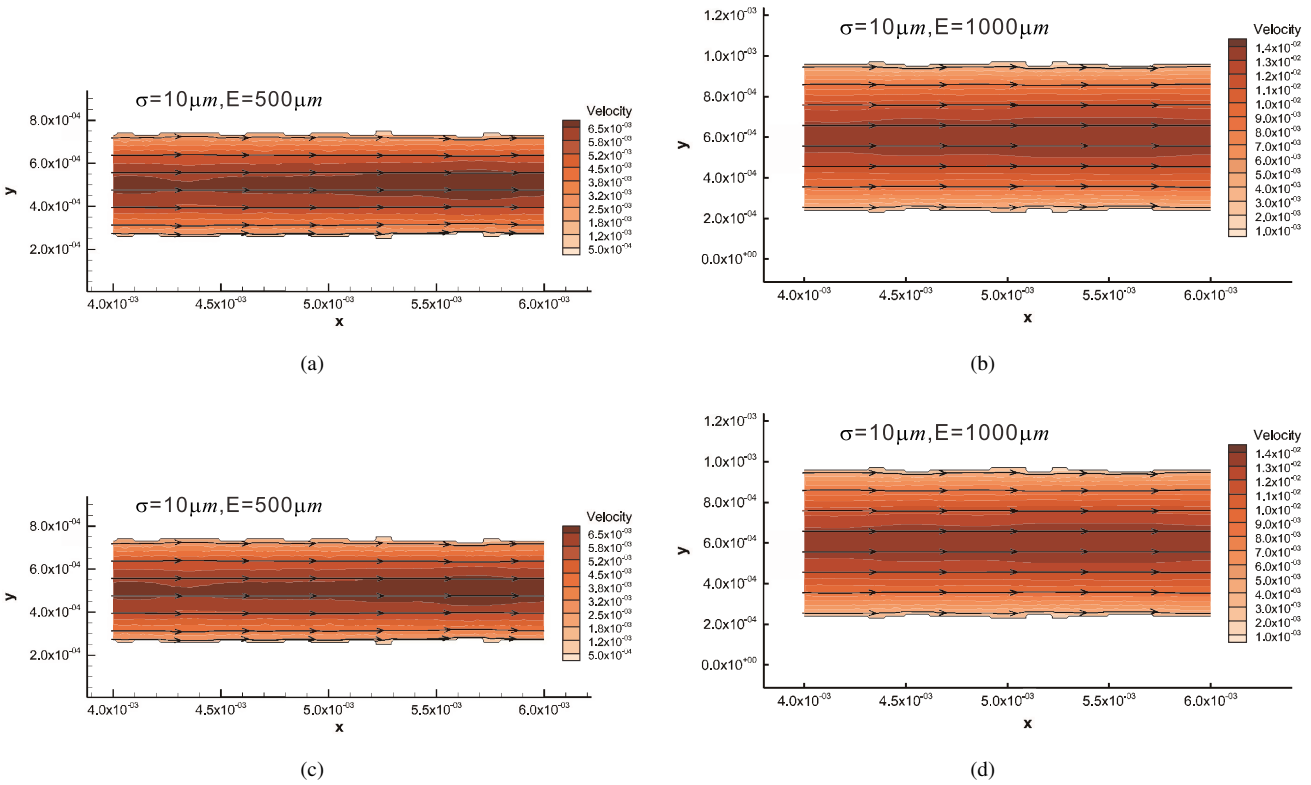

Fig. 4. The flow pattern in fractures with different E, selecting case 1 as an example.

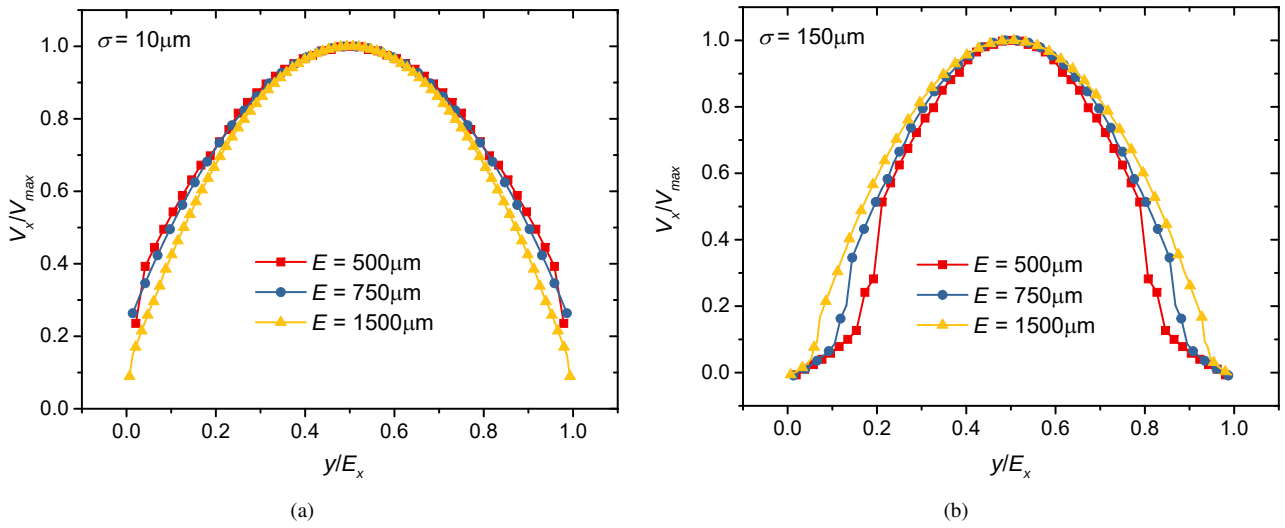

Fig. 5. Velocity distribution profiles at x/L = 0.55. (a) a relatively smooth fracture; (b) a very rough fracture.

smooth fracture, the alteration is not evident.

When we extract the sectional velocity profile at x/L = 0.55, it is clear to see that the velocity distribution differs with σ and E (Fig. 5). For a relatively smooth fracture, the dimensionless velocity (V_x/V_{max}) near boundary increases with the decrease of E, which means the microflow effect is evident in smooth fractures, as shown by Fig. 5(a). However, V_x/V_{max} near the boundary decreases with the reduction on E in Fig. 5(b), which is a very rough fracture case. Definitely, for this case, the roughness effect has greater impacts on fracture flow and the microflow effect is not evident. Comparing two cases, it concludes that two important effects of the microflow in rough fractures, the microflow effect and the roughness effect, compete with each other when E changes.

As the flow is driven by pressure gradient, the flow rate may sensitively response to slight differences on pressure distribution. Fig. 6 presents pressure distribution profiles along the flow direction of two kinds of fractures. For a relatively smooth fracture, the pressure distribution curve is close to linear and the deviation from the validation group is almost

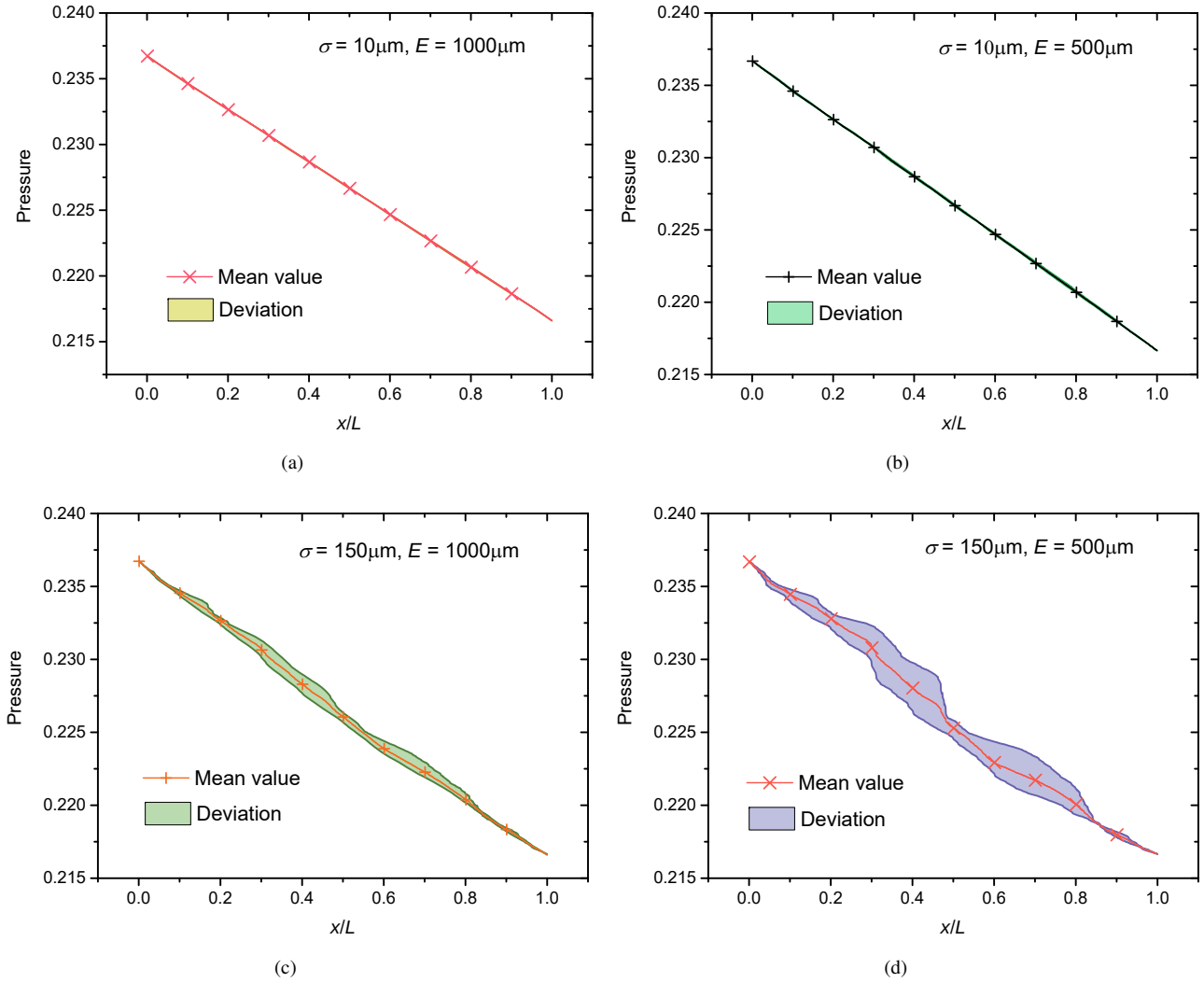

Fig. 6. Pressure distribution profiles along the flow direction in fractures with different E.

zero. In addition, the curve stays nearly constant as E changes. For a rough fracture, the pressure distribution curve is also nearly linear when E is large. With the decreasing of E, the curve becomes torturous and nonlinear. The deviation is also enlarged. The resultant stresses that the roughness effect is enhanced by small apertures and definitely reduces flow rate accordingly.

4.2 The hybrid role of E and σ

Based on the above analysis, we try to figure out the influence of the microflow effect, which is directly controlled by E, and the roughness effect, which is explicitly represented by σ. As E decreases, the microflow effect is enhanced, intuitively expressed by an increase on $\overline{Kn}$. The roughness effect is also strengthened by the decrease of E, expressing with the increase of σ/E. These two effects compete with each other and finally, the combined effects are reflected by flow rate.

As Fig. 7 shows, results from numerical simulation and modified empirical models both present two trends. For a smooth fracture, e/E decreases with the increase of E (as Fig. 7(a) shows). All of the modified empirical models correctly predict this trend and the one based on the Rasouli and Hosseinian's (2011) is very close to the numerical result. In this case, the microflow effect dominates the flow behavior and it abates when E is enlarged.

Nevertheless, for a rough fracture, the simulation result indicates that e/E rises with the increase of E, and modified models separate into two groups (see Fig. 7(b)). Most of the modified models show a declining trend on the curve and the data provided by them are very similar. However, as shown by our numerical results, the ratio increases for the rough fracture case. Only one modified model based on Rasouli and Hosseinian's provides a good prediction on this trend. Due to parameters of their empirical model was established from data of three-dimensional examples, it shows a larger predicting value on e/E than ours. This finding indicates that as the scaling down of E, the roughness effect is dominant on flow in very rough fractures.

In order to achieve a comprehensive understanding of this phenomenon, more cases are taken into our research. With σ

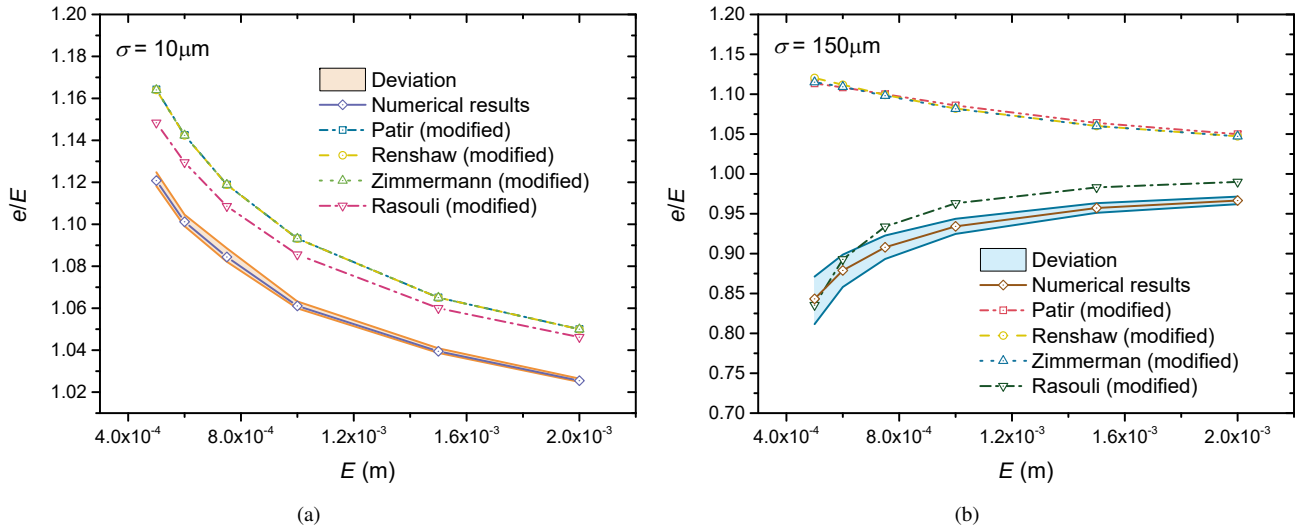

(a) (b)

Fig. 7. Comparison of e/E between the numerical result and modified empirical models (with cases of both very rough and relatively smooth fractures).

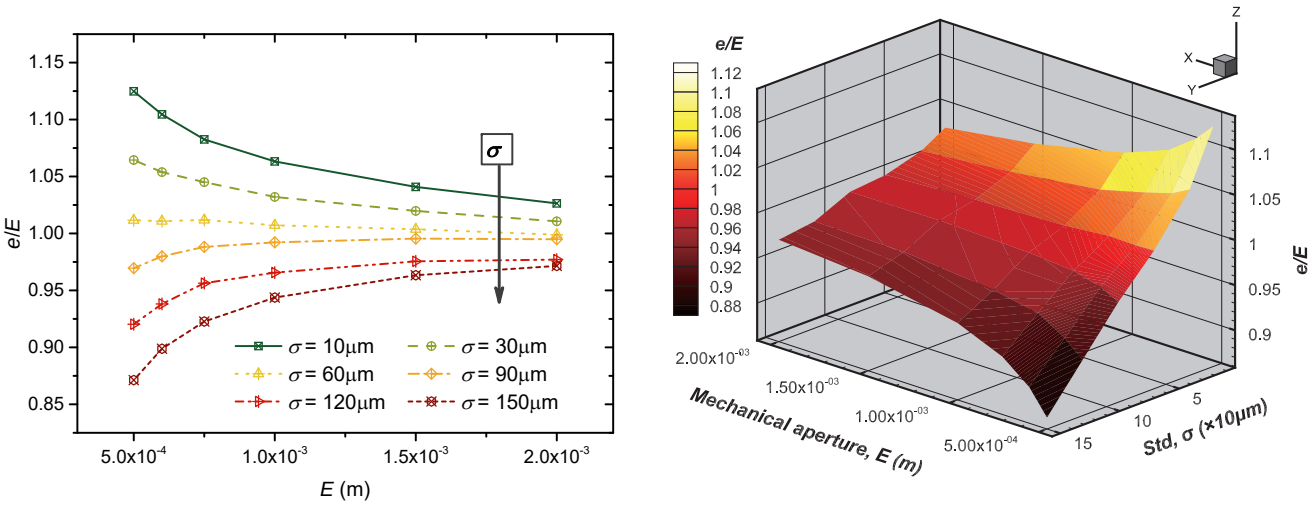

(a) (b)

Fig. 8. The relationship between e, E, and σ under the condition of microflow in rough fractures.

varies from 10 to 150 μm and E varies from 500 to 2000 μm, additional 36 examples are simulated to make compensation to a more detailed relationship between e/E, σ and E. Both a 2D graph and a 3D diagram are shown in Fig. 8. The trend of the relationship between e/E and E is changeable. For rougher cases with high σ, the trend is downward, but for smoother cases, the trend is upward. There also exists an equilibrium point between the microflow effect and the roughness effect, when the value of σ is close to 60 μm. After interpolating the missing data, Fig. 8(b) presents a full scene of the relationship quantitatively.

5. Summary

The behavior of microflow through rough fractures is affected both by the microflow effect and the roughness effect. To obtain a better understanding of this issue, analytical research is conducted and a lattice Boltzmann method code is used to simulate the microflow through 2D fractures.

Theoretical analysis roughly shows the relationship between e/E, σ/E and $\overline{Kn}$, based on modified forms of previous empirical models which already contain roughness effect. With the change of E, competitive relationship between the microflow effect and the roughness effect is shown analytically.

Numerical investigations are carried out on artificially generated 2D fractures with random roughness following Gaussian distribution. Through analysis of the flow field, different modes of velocity change are shown, which is caused by the scaling down of E. Numerical results also show different trends on the relationship between e/E and E for rough-fracture cases and smooth-fracture cases. Further research shows a clear pattern on the relationship between σ, E, and

e/E. For rough cases, e/E rises with the increase of E, but for relatively smooth cases, e/E declines with the increase of E. Equilibrium point is also found from the simulation, whose value of σ is approximately 60 μm. The result gives guidance on the prediction of e and clearly reveals the mechanism of the microflow effect and the roughness effect on microflow through rough fractures. However, due to the simplification of 2D models, investigations based on 3D fractures is needed when considering engineering application.

Nomenclature

$\widetilde{Q}$ = Flow rate of the fracture, m^3/s
μ = Dynamic viscosity, Pa·s
ν = Kinematic viscosity, m^2/s
e = Hydraulic aperture, m
e_r = Modified aperture with roughness, m
E = Mechanical aperture, m
E_x = Local aperture, m
p = Pressure, Pa
∇p = Pressure gradient, Pa/m
σ = Standard deviation of the aperture, m
λ = Mean free path of fluid molecules, m
L = Characteristic length, m
Kn = Knudsen number ($\equiv \lambda/L$)
$\widehat{Kn}$ = Kn defined by hydraulic aperture
$\overline{Kn}$ = Mean Kn of the fracture
ρ = Fluid density, kg/m^3
$\mathbf{u}$ = Flow velocity, m/s
$\mathbf{e}_i$ = Discretized velocity at direction i, m/s
f_i = Discrete particle velocity distribution function
f_i^{eq} = Discrete local equilibrium velocity distribution function
$\mathbf{r}$ = Position, m
Δx = Space step, m
t = Time, s
Δt = Time step, s
c = Characteristic speed of lattice ($\equiv \Delta x/\Delta t$), m/s
N_E = Number of grids for mechanical aperture
ζ = Random number ranging between 0.0 and 1.0

Acknowledgments

We express our gratitude for an eternal friend Prof. Guangcai Zhang at IAPCM, who had devoted all his life to a scientific career. We wish to thank Prof. Lanru Jing and Dr. Liangchao Zou for helpful discussions. This work is supported by the National Natural Science Foundation of China (under Grant Nos. 11772064, 51727807, and 41472130) and CAEP Foundation (Grant No. CX2019033).

References

Ansumali, S., Karlin, I.V. Kinetic boundary conditions in the lattice Boltzmann method. Phys. Rev. E 2002, 66(2): 026311.

Barton, N., Choubey, V. The shear strength of rock joints in theory and practice. Rock Mech. 1977, 10(1-2): 1-54.

Boutt, D.F., Grasselli, G., Fredrich, J.T., et al. Trapping zones: The effect of fracture roughness on the directional anisotropy of fluid flow and colloid transport in a single fracture. Geophys. Res. Lett. 2006, 33(21): L21402.

Brown, S.R. Simple mathematical model of a rough fracture. J. Geophys. Res. Sol. Ea. 1995, 100(B4): 5941-5952.

Cacas, M.C., Ledoux, E., Marsily, G.D., et al. Modeling fracture flow with a stochastic discrete fracture network: Calibration and validation: 1. The flow model. Water Resour. Res. 1990, 26(3): 479-489.

Cai, J., Yu, B., Zou, M., et al. Fractal analysis of surface roughness of particles in porous media. Chinese Phys. Lett. 2010, 27(2): 024705.

Ciezobka, J., Courtier, J., Wicker, J. Hydraulic fracturing test site (HFTS)-Project overview and summary of results. Paper URTEC2937168 Presented at the Unconventional Resources Technology Conference, Houston, Texas, USA, 23-25 July, 2018.

Darabi, H., Ettehad, A., Javadpour, F., et al. Gas flow in ultra-tight shale strata. J. Fluid Mech. 2012, 710: 641-658.

Eker, E., Akin, S. Lattice Boltzmann simulation of fluid flow in synthetic fractures. Transp. Porous Media 2006, 65(3): 363-384.

Golparvar, A., Zhou, Y., Wu, K., et al. A comprehensive review of pore scale modeling methodologies for multiphase flow in porous media. Adv. Geo-Energy Res. 2018, 2(4): 418-440.

Karniadakis, G., Beskok, A., Aluru, N. Microflows and Nanoflows: Fundamentals and Simulation. New York, Springer Science & Business Media, 2006.

Li, J., Ho, M.T., Wu, L., et al. On the unintentional rarefaction effect in LBM modeling of intrinsic permeability. Adv. Geo-Energy Res. 2018, 2(4): 404-409.

Liu, H., Zhang, X., Lu, X., et al. Study on flow in fractured porous media using pore-fracture network modeling. Energies 2017, 10(12): 1984.

Liu, R., Jiang, Y., Huang, N., et al. Hydraulic properties of 3D crossed rock fractures by considering anisotropic aperture distributions. Adv. Geo-Energy Res. 2018, 2(2): 113-121.

Louis, C. Rock hydraulics, in Rock Mechanics, edited by L. Müller, Vienna, Springer, pp. 299-387, 1972.

Luo, S., Zhao, Z., Peng, H., et al. The role of fracture surface roughness in macroscopic fluid flow and heat transfer in fractured rocks. Int. J. Rock Mech. Min. 2016, 87: 29-38.

Myers, N. Characterization of surface roughness. Wear 1962, 5(3): 182-189.

Oron, A.P., Berkowitz, B. Flow in rock fractures: The local cubic law assumption reexamined. Water Resour. Res. 1998, 34(11): 2811-2825.

Patir, N., Cheng, H. An average flow model for determining effects of three-dimensional roughness on partial hydrodynamic lubrication. J. Lubr. Technol. 1978, 100(1): 12-17.

Rasouli, V., Hosseinian, A. Correlations developed for estimation of hydraulic parameters of rough fractures

through the simulation of JRC flow channels. Rock Mech. Rock Eng. 2011, 44(4): 447-461.

Renshaw, C.E. On the relationship between mechanical and hydraulic apertures in roughwalled fractures. J. Geophys. Res. Sol. Ea. 1995, 100(B12): 24629-24636.

Succi, S. The Lattice Boltzmann Equation: For Fluid Dynamics and Beyond. New York, USA, Oxford University Press, 2001.

Tang, G., Tao, W., He, Y. Lattice Boltzmann method for gaseous microflows using kinetic theory boundary conditions. Phys. Fluids 2005, 17(5): 058101.

Wang, M., Chen, Y., Ma, G., et al. Influence of surface roughness on nonlinear flow behaviors in 3D self-affine rough fractures: Lattice Boltzmann simulations. Adv. Water Resour. 2016, 96: 373-388.

Wang, Z., Wang, M., Chen, S. Coupling of high Knudsen number and non-ideal gas effects in microporous media. J. Fluid Mech. 2018, 840: 56-73.

Witherspoon, P.A., Wang, J.S., Iwai, K., et al. Validity of cubic law for fluid flow in a deformable rock fracture. Water Resour. Res. 1980, 16(6): 1016-1024.

Xu, A., Gonnella, G., Lamura, A. Phase-separating binary fluids under oscillatory shear. Phys. Rev. E 2003, 67(5): 056105.

Xu, A., Gonnella, G., Lamura, A., et al. Scaling and hydrodynamic effects in lamellar ordering. EPL-Europhys. Lett. 2005, 71(4): 651.

Xu, A., Gonnella, G., Lamura, A. Simulations of complex fluids by mixed lattice Boltzmann-finite difference methods. Phys. A 2006a, 362(1): 42-47.

Xu, A., Gonnella, G., Lamura, A. Morphologies and flow patterns in quenching of lamellar systems with shear. Phys. Rev. E 2006b, 74(1): 011505.

Zhang, G., Feng, C., Gong, W., et al. Simulation and analysis of the effect of roughness elements on fluid flow through single fracture based on lattice Boltzmann method. Scientia Sinica Physica, Mechanica & Astronomica 2017, 47(2): 024701. (in Chinese)

Zhang, G., Tian, Y., Li, Y. Numerical study on the mechanism of fluid flow through single rough fractures with different JRC. Scientia Sinica Physica, Mechanica & Astronomica 2018b, 49(1): 014701. (in Chinese)

Zhang, Y., Xu, A., Zhang, G., et al. Discrete Boltzmann method with Maxwell-type boundary condition for slip flow. Commun. Theor. Phys. 2018a, 69(1): 77.

Zhao, J., Yao, J., Li, A., et al. Simulation of microscale gas flow in heterogeneous porous media based on the lattice Boltzmann method. J. Appl. Phys. 2016, 120(8): 084306.

Zhao, Z., Li, B. On the role of fracture surface roughness in fluid flow and solute transport through fractured rocks. Paper ISRM-13CONGRESS-2015-051 Presented at the 13th ISRM International Congress of Rock Mechanics, Montreal, Canada, 10-13 May, 2015.

Zhao, Z., Peng, H., Wu, W., et al. Characteristics of shear-induced asperity degradation of rock fractures and implications for solute retardation. Int. J. Rock Mech. Min. 2018, 105: 53-61.

Zhou, J., Wang, M., Wang, L., et al. Emergence of nonlinear laminar flow in fractures during shear. Rock Mech. Rock Eng. 2018, 51(11): 3635-3643.

Zimmerman, R.W., Bodvarsson, G.S. Hydraulic conductivity of rock fractures. Transp. Porous Media 1996, 23(1): 1-30.

Zimmerman, R.W., Kumar, S., Bodvarsson, G. Lubrication theory analysis of the permeability of rough-walled fractures. Berkeley, Lawrence Berkeley National Laboratory, 1991.

Zou, L., Jing, L., Cvetkovic, V. Roughness decomposition and nonlinear fluid flow in a single rock fracture. Int. J. Rock Mech. Min. 2015, 75: 102-118.

Zou, Q., He, X. On pressure and velocity boundary conditions for the lattice Boltzmann BGK model. Phys. Fluids 1997, 9(6): 1591-1598.

Appendix

Table A-1. Physical parameters for the simulation.

Parameters	Physical value
Grid step	1×10^{-5} m
Time step	1×10^{-5} s
Fluid density	0.65 kg/m^3
Kinematic viscosity	1.80×10^{-5} m^2/s
Pressure gradient	2 Pa/m

Table A-2. The expression of empirical models for hydraulic aperture.

References	Expressions
Patir and Cheng, 1978	$\frac{e}{E}=\left[1-0.9\exp\left(-0.56\frac{E}{\sigma}\right)\right]^{\frac{1}{3}}$
Renshaw, 1995	$\frac{e}{E}=\left(1+\frac{\sigma^2}{E^2}\right)^{-\frac{1}{2}}$
Zimmerman and Bodvarsson, 1996	$\frac{e}{E}=\left(1-1.5\frac{\sigma^2}{E^2}+\ldots\right)^{\frac{1}{3}}$
Rasouli and Hosseinian, 2011	$\frac{e}{E}=\left(1-2.25\frac{\sigma}{E}\right)^{\frac{1}{3}}$